Hadronic Υ production, parton distributions, and quantum chromodynamics

J. F. Owens and E. Reya*
Department of Physics, Florida State University, Tallahassee, Florida 32306
(Received 3 November 1977)

Using the combined version of light-quark ($q\bar{q} \to b\bar{b}$) and gluon-gluon ($gg \to b\bar{b}$) fusion mechanisms for hadronic $\Upsilon(9.5)$ production, we give predictions for x_F distributions using pion and proton beams, and for various total-cross-section beam ratios. In addition, we make a detailed comparison of counting-rule–like nucleonic and pionic parton distributions with those predicted by dynamical quantum-chromodynamics (QCD) calculations, and give analytic parametrizations of their QCD x and Q^2 dependence.

I. INTRODUCTION

The recently discovered[1] resonance, $\Upsilon(9.5)$, in the mass spectrum of dimuons produced in 400-GeV proton-nucleus collisions suggests the existence of at least one new quark flavor.[2,3] The simplest model which could incorporate such quarks is a six-quark generalization[4] of the standard Weinberg-Salam SU(2)⊗U(1) model in which the new quarks, t and b, form a left-handed doublet. Using the same hadronic production mechanism for the Υ as for the J/ψ, theoretical estimates[3,5] show a slight preference for the Υ to be a $b\bar{b}$ state rather than a $t\bar{t}$ state. For definiteness we shall accept the $b\bar{b}$ interpretation of the $\Upsilon(9.5)$.

We have recently demonstrated[6] the necessity of including the gluon-gluon annihilation process in addition to the usual (light) quark fusion model[7] for explaining hadronic J/ψ production: The subprocess $q\bar{q} \to c\bar{c}$, where $q = u, d, s$, is not sufficient to account for the x_F distributions and various beam ratios of J/ψ production cross sections measured at CERN SPS and Fermilab. The success with the ψ's encourages us to apply these combined hadronic production mechanisms also to the Υ, i.e., to study the effects of $q\bar{q} \to b\bar{b}$ subprocesses in the lowest order of quantum chromodyanmics (QCD). We will mainly concentrate on predictions for x_F distributions using proton as well as pion beams, and for the ratios of various total Υ-production cross sections using p, $\bar{p}$, $\pi^{\pm}$, and $K^{\pm}$ beams.

Before presenting these results we recall our assumptions about quark and gluon distributions which, for $\Upsilon(9.5)$ production, are tested at $Q^2 \simeq 100\ \mathrm{GeV}^2$ where QCD effects are important. The numerical calculations are greatly facilitated by using simple parametrizations of the parton distributions for their x as well as Q^2 dependence as predicted by QCD. Since we will use two different (extreme) sets of nucleonic and pionic parton distributions, we first briefly discuss in Sec. II how these parametrizations were obtained. The two sets of parton distributions in question refer to either counting-rule–like distributions[8] corrected by the QCD Q^2 dependence or to dynamically[9,10] calculated QCD distributions. In Sec. III we present our predictions for Υ-production cross sections using p, $\bar{p}$, $\pi^{\pm}$, and $K^{\pm}$ beams.

II. PARTON DISTRIBUTIONS

Predictions for J/ψ and Υ production based on the sum of $q\bar{q}$ and gg production mechanisms clearly are dependent on the specific parton distributions used. In this analysis we have chosen to use two types of distributions which yield approximate upper and lower estimates of the gluon content in pions and protons. The counting-rule[8] distributions give generous estimates for the gluon and sea quark functions at low values of Q^2. On the other hand, the dynamically calculated distributions[9,10] give smaller estimates for the sea quark and gluon distributions in the vicinity of $Q^2 = Q_0^2$. Comparing the predictions which result from the use of these different distributions gives some insight as to the model dependency of the various predictions. In this section the various pion and nucleon distribution functions are discussed in detail. For the actual numerical calculations, it was convenient to employ parametrizations of the various x and Q^2 dependent functions. In each instance the distributions were calculated for a range in x and Q^2 and then fitted with simple functional forms. For completeness, we have included the parametrizations which we used.

A. Counting-rule–like distributions

One set of distributions we shall use is based on counting-rule–like[8] input distributions at $Q^2 = Q_0^2$. As far as the Q^2 dependence of nucleonic distributions is concerned we follow closely the parametrizations suggested by Buras and Gaemers.[11] Using the common decomposition

$u = u_v + \xi$, $d = d_v + \xi$, and $\bar{u} \simeq \bar{d} \simeq s \simeq \bar{s} \equiv \xi$ (for the present purpose all contributions stemming from the charmed sea are negligible), we keep the same lowest moments as in Ref. 11, i.e.,

$$\begin{aligned} &\langle x u_v(Q_0^2) + x d_v(Q_0^2)\rangle_2 = 0.488 \ , \\ &\langle x \xi(Q_0^2)\rangle_2 = 0.0183 \ , \\ &\langle x G(Q_0^2)\rangle_2 = 0.402 \ , \end{aligned} \tag{1}$$

with $Q_0^2 = 1.8$ GeV^2 and where the moments are defined by

$$\langle f(Q^2)\rangle_n \equiv \langle f(x,Q^2)\rangle_n \equiv \int_0^1 dx x^{n-2} f(x,Q^2) \ .$$

Furthermore, we have chosen the x dependence of the input sea and gluon distributions to be in agreement with naive counting rules,[8] i.e.,

$$x\xi(x,Q_0^2) = 0.147(1-x)^7, \quad xG(x,Q_0^2) = 2.412(1-x)^5 \ . \tag{2}$$

The full Q^2 dependence for the valence part is then given by the parametrization of Ref. 11, which has been obtained by fitting the first 12 moments predicted by QCD:

$$x u_v(x,Q^2) + x d_v(x,Q^2) = \frac{3}{B(\eta_1, 1+\eta_2)} x^{\eta_1}(1-x)^{\eta_2} \ , \tag{3}$$

$$x d_v(x,Q^2) = \frac{1}{B(\eta_3, 1+\eta_4)} x^{\eta_3}(1-x)^{\eta_4} \ , \tag{4}$$

with

$$\begin{aligned} &\eta_1 = 0.7 - 0.176\bar{s}, \quad \eta_2 = 2.6 + 0.80\bar{s} \ , \\ &\eta_3 = 0.85 - 0.24\bar{s}, \quad \eta_4 = 3.35 + 0.816\bar{s} \ , \end{aligned}$$

where $\bar{s} = \ln[\ln(Q^2/\Lambda^2)/\ln(Q_0^2/\Lambda^2)]$, $Q_0^2 = 1.8$ GeV^2, and $\Lambda \simeq 0.5$ sets the scale of the strong-interaction coupling constant.[12] The use of Euler beta functions, $B(\eta_i, 1+\eta_{i+1})$, $i = 1, 3$, ensures baryon number conservation for all values of Q^2.[11] In order to obtain the Q^2 dependence for the sea and gluon densities of Eq. (2) we have Mellin-inverted the appropriate moments predicted by QCD, and fitted these predictions using the following parametrizations:

$$x\xi(x,Q^2) = A_s(1-x)^{\eta_s} + A_s'(1-x)^{\eta_s'} + B_s e^{-C_s x} \ , \tag{5}$$

$$xG(x,Q^2) = A_g(1-x)^{\eta_g} + A_g'(1-x)^{\eta_g'} + B_g e^{-C_g x} \ , \tag{6}$$

with

$$\begin{aligned} A_i &= A_i^{(0)} + A_i^{(1)}\bar{s} + A_i^{(2)}\bar{s}^2 \ , \\ \eta_i &= \eta_i^{(0)} + \eta_i^{(1)}\bar{s} + \eta_i^{(2)}\bar{s}^2 \ , \\ A_i' &= A_i'^{(1)}\bar{s} + A_i'^{(2)}\bar{s}^2 \ , \\ \eta_i' &= \eta_i'^{(0)} + \eta_i'^{(1)}\bar{s} + \eta_i'^{(2)}\bar{s}^2 \ , \\ B_i &= B_i^{(1)}\bar{s} + B_i^{(2)}\bar{s}^2 \ , \\ C_i &= C_i^{(0)} + C_i^{(1)}\bar{s} + C_i^{(2)}\bar{s}^2 \ , \end{aligned} \tag{7}$$

where the fitted expansion coefficients are given in Table I. These parametrizations are valid for $x \gtrsim 0.02$ and $0 \leq s \lesssim 1.6$. The somewhat unconventional form utilized in Eqs. (5) and (6) was chosen in order to reproduce the dramatic peaking at low x values which is characteristic of QCD predictions for $Q^2 \gg Q_0^2$. The exponential term is negligible

TABLE I. Values for the parameters defined by the power-series expressions in Eq. (7) for the QCD parametrizations of sea and gluon distributions. For the dynamical QCD predictions one has to take $\bar{s} \to \bar{s} + \ln L_0$ as explained in the text.

	Counting rule				Dynamical QCD			
	$x\xi$	xG	$x\xi^\pi$	xG^π	$x\xi$	xG	$x\xi^\pi$	xG^π
$A^{(0)}$	0.1467	2.4120	0.1	2.0	0.0	0.0	0.0	0.0
$A^{(1)}$	−0.1211	−1.9845	−0.0676	−1.9551	0.0227	0.3125	0.0087	0.1989
$A^{(2)}$	0.0274	0.4443	0.0172	0.5096	−0.0045	−0.0560	−0.0011	−0.0376
$A'^{(1)}$	0.1853	3.6363	0.1613	3.7892	0.0389	0.9237	0.0137	0.6107
$A'^{(2)}$	−0.0608	−1.4146	−0.0508	−1.7836	−0.0011	−0.1021	0.0032	−0.0707
$\eta^{(0)}$	7.0	5.0	5.0	3.0	4.8726	1.4265	1.1044	−0.2507
$\eta^{(1)}$	0.0217	1.5464	−0.2647	1.4445	0.3428	1.4483	0.9957	1.3088
$\eta^{(2)}$	0.0037	−0.5287	0.3376	−0.5852	0.1015	−0.0142	−0.0165	−0.0702
$\eta'^{(0)}$	9.5041	13.8237	6.5329	6.5772	10.9605	1.8769	0.5377	−1.1338
$\eta'^{(1)}$	1.0165	0.7914	1.7012	4.7147	1.2669	2.5026	3.0924	3.2339
$\eta'^{(2)}$	−0.1049	−0.2873	0.0600	−1.9628	0.0011	0.4152	−0.0701	−0.0451
$B^{(1)}$	0.1682	7.6609	0.1442	8.1246	−0.0100	2.7120	0.0231	2.3634
$B^{(2)}$	0.4473	−1.4595	0.0508	−2.0240	0.0481	−0.0145	0.0270	−0.0919
$C^{(0)}$	25.8997	36.7928	29.4902	57.8632	29.9236	29.2319	8.6310	32.1351
$C^{(1)}$	3.9572	12.5884	3.8843	−24.4474	3.8858	−3.3769	9.9432	−6.6125
$C^{(2)}$	1.6331	−1.1536	0.5861	8.6888	1.0451	3.6739	0.1253	2.9788

outside the small x region, as can be seen from the large values for C_s and C_g given in Table I.

The results of this procedure differ from those obtained using the prescription of Ref. 11, where only the $n=2$ and 3 moments were taken into account in order to obtain parametrizations for $x\xi(x,Q^2)$ and $xG(x,Q^2)$ in the region $x \lesssim 0.3$. In Fig. 1 we compare this parametrization technique for $Q^2=100$ GeV^2 (dotted curves) with our parametrization (long-dashed curves) obtained from the exactly inverted moments. The agreement for the sea is reasonable but becomes worse for the (flatter) gluon: The parametrization technique of Buras and Gaemers[11] strongly overestimates the Q^2 dependence by predicting the gluon density to be about a factor of 2 too small at $x \simeq 0.3$ and twice as large as the exact QCD prediction at $x \simeq 0.1$. This discrepancy becomes even worse for input densities with lower powers of $(1-x)$, as for pionic distributions, since for an input behaving like $(1-x)^d$, its nth moment vanishes like $1/n^{d+1}$ for $n \to \infty$.

The pionic counting-rule–like[8] valence, sea, and gluon input distributions at $Q^2=Q_0^2=3$ GeV^2 are given by

$$xv^{\pi}(x,Q_0^2)=\tfrac{3}{4}\sqrt{x}\,(1-x)\ , \tag{8}$$

$$x\xi^{\pi}(x,Q_0^2)=0.1(1-x)^5\ ,$$

$$xG^{\pi}(x,Q_0^2)=2(1-x)^3\ , \tag{9}$$

which satisfy the total-momentum-conservation sum rule as well as the baryon-number constraint $\langle xv^{\pi}(Q^2)\rangle_1=1$. Here we have used the conventional decomposition

$$u^{\pi^+}=\bar{d}^{\pi^+}=\bar{u}^{\pi^-}=d^{\pi^-}=v^{\pi}+\xi^{\pi}\ ,$$

$$\bar{u}^{\pi^+}=d^{\pi^+}=u^{\pi^-}=\bar{d}^{\pi^-}\simeq s^{\pi^\pm}=\bar{s}^{\pi^\pm}\equiv\xi^{\pi}\ .$$

Proceeding in the same way as for nucleons, the valence term was parametrized as

$$xv^{\pi}(x,Q^2)=\frac{1}{B(\eta_1^{\pi},1+\eta_2^{\pi})}\,x^{\eta_1^{\pi}}(1-x)^{\eta_2^{\pi}}\ . \tag{10}$$

The parameters in Eq. (10) were determined by fitting the first 12 moments, calculated with Eqs. (8) and (9) as input, yielding

$$\eta_1^{\pi}=0.5-0.103\sqrt{\bar{s}}\ \text{ and }\ \eta_2^{\pi}=1+0.691\bar{2}s\ ,$$

valid up to $\bar{s}\simeq 1.6$. The pionic gluon and sea distributions are given by the same analytic expressions as in Eqs. (5)–(7). The parameters were determined by fitting the distributions obtained by the Mellin inversion of the QCD predicted moments. The resulting parameter values are given in Table I. In Fig. 2 the QCD predictions at $Q^2=100$ GeV^2 (long dashed curves) are compared with the results obtained using the approximation technique of Buras and Gaemers[11] based on the use of $n=2$ and 3 moments only (dotted curves). As noted previously, this latter parametrization technique is unable to describe the detailed x dependence of the sea and gluon distributions. Thus for processes which depend sensitively on the detailed x dependence of the sea and gluon distributions, it could be misleading to use the parametrizations of Ref. 11.

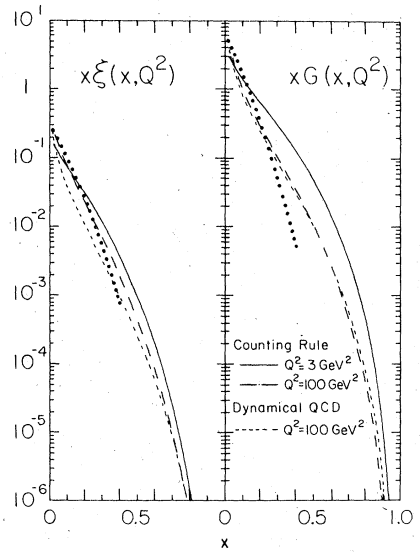

FIG. 1. The counting-rule nucleon sea and gluon distributions at $Q^2=3$ GeV^2 (solid line) and 100 GeV^2 (long dashed line). For comparison the corresponding parametrizations, obtained using the ansatz of Ref. 11, are shown at $Q^2=100$ GeV^2 (dotted line). The dynamical QCD distributions at $Q^2=100$ GeV^2 are shown by the short dashed lines.

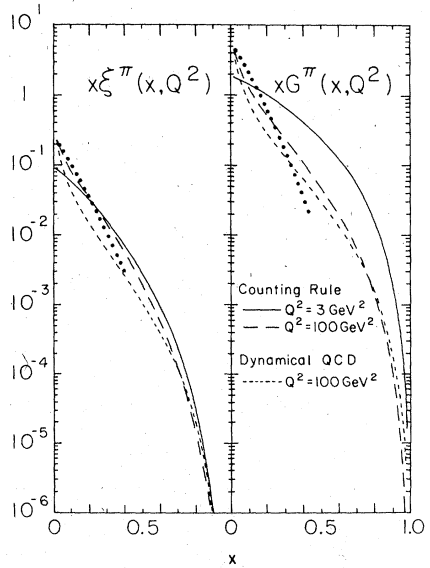

FIG. 2. The various sea and gluon distributions for the pion with the same notation as in Fig. 1.

B. Dynamical QCD distributions

The other set of parton distributions used correspond to the dynamically[9] calculated QCD predictions.[10] These are obtained, with the help of well-known renormalization-group techniques, by assuming that at low-resolution energies, $Q^2=\mu^2$, hadrons consist of valence quarks only, i.e., $x\xi(x,\mu^2)=xG(x,\mu^2)=0$. Parametrizations for the resulting nucleonic distributions valid up to $Q^2 \simeq 200$ GeV^2 are given in Ref. 10. For completeness we have refitted the exactly inverted dynamical QCD moments[10] using similar parametrizations as before in order to obtain expressions valid in a much larger Q^2 range. The two valence distributions are parametrized as

$$xu_v(x,Q^2)=x^{\eta}\sum_{i=1}^{4}A_i(1-x)^{\eta i}\ , \tag{11}$$

with $\eta=0.5+0.0034\bar{s}-0.02005\bar{s}^2$ and

$$\begin{aligned} &A_1=5.496,\quad A_2=-3.844\ ,\\ &A_3=-0.822,\quad A_4=0.450\ ,\\ &\eta_1=3+0.798\bar{s},\quad \eta_2=5-0.384\bar{s}\ ,\\ &\eta_3=7+34.5\bar{s},\quad \eta_4=9-3.381\bar{s}, \end{aligned} \tag{12}$$

where $\bar{s}$ is calculated with $Q_0^2=3$ GeV^2 and $\Lambda=0.5$ GeV. The "static point" at which nucleons consist of valence quarks only is given by[10] $L_0\equiv\ln(Q_0^2/\Lambda^2)/\ln(\mu^2/\Lambda^2)\simeq 7$. Similarly, $xd_v(x,Q^2)$ is represented by the same analytic expression as given in Eq. (11), but with $\eta=0.5-0.1017\bar{s}+0.0139\bar{s}^2$ and

$$\begin{aligned} &A_1=2.332,\quad A_2=1.907,\\ &A_3=-3.657\ ,\quad A_4=0.774\ ,\\ &\eta_1=4+0.973\bar{s},\quad \eta_2=5+1.383\bar{s},\\ &\eta_3=7-0.389\bar{s},\quad \eta_4=9-2.042\bar{s}\ . \end{aligned} \tag{13}$$

The sea and gluon distributions are parametrized as in Eqs. (5)–(7) with the parameters given in Table I. All these representations are valid for $x\gtrsim 0.02$ and $0\leq\bar{s}\lesssim 1.6$. In Fig. 1 we compare these dynamically calculated sea and gluon distributions (short-dashed curves) at $Q^2=100$ GeV^2 with the ones obtained from using the (flat) counting-rule-like input distributions (long-dashed curves). Although at $Q^2=3$ GeV^2 the counting-rule–like input distributions, Eq. (2), are much flatter than the dynamical predictions,[10] they reduce very quickly to the shape and size of the dynamically calculated densities at higher values of Q^2. At $Q^2=100$ GeV^2 the originally flat counting-rule gluon has developed a sharp peak at small x due to having pair created the sea, and is almost indistinguishable from the dynamical QCD prediction as can be seen in Fig. 1. The dynamical sea distribution underestimates the counting-rule sea by at most a factor of 2 in the intermediate x range at $Q^2=100$ GeV^2 and, as shown in Fig. 1, the two distributions coincide at small x.

In order to obtain the pionic parton distributions we only have to use Eq. (8) as input at $Q_0^2=3$ GeV^2 $\gg\mu^2$ which fixes[10] the moments for $x\xi^{\pi}$ and xG^{π} once the "static" point μ^2 is specified. This latter quantity, or equivalently $L_0\equiv\ln(Q_0^2/\Lambda^2)/\ln(\mu^2/\Lambda^2)$, is then determined by imposing total-momentum conservation, i.e.,

$$1=\langle 2xv^{\pi}(\mu^2)\rangle_2=\tfrac{2}{5}e^{(32/81)\ln L_0}\ ,$$

which yields $L_0\simeq 10$. The full Q^2 dependence of the valence density is then given by the same parametrization as in Eq. (10), whereas the predictions for the pionic gluon and sea distributions can be parametrized by the same analytic expressions as in Eqs. (5)–(7) with $\bar{s}\to\bar{s}_d=\bar{s}+\ln 10$ and with the parameters given in Table I. Again these parametrizations are valid for $x\gtrsim 0.02$ and $0\leq\bar{s}\lesssim 1.6$. In Fig. 2 we compare the dynamical predictions (short-dashed curves) for the sea and gluon content in the pion with the counting-rule–like parametrizations (long-dashed curves) at $Q^2=100$ GeV^2. The dynamical predictions might underestimate these distributions by at most a factor of 2 in the intermediate x range, and coincide with the counting-rule–like distributions for small values of x—a situation very similar to the nucleon case. Therefore, in contrast to common belief, the use of dynamically calculated QCD parton distributions does not heavily underestimate the sea and gluon content of hadrons if they are probed at resolution energies sufficiently above the typical input values of $Q^2=Q_0^2\simeq 3$ GeV^2.

III. Υ PRODUCTION

Having fixed the two sets of parton distributions, which are in good agreement,[9-11,13] with the present deep-inelastic lepton-nucleon data, we now can predict (up to an overall normalization) the Υ x_F distributions, cross-section beam ratios, and cross-section energy dependences using the well known hadronic Drell-Yan mechanism with the[7] $q\bar{q}\to b\bar{b}$ and[6] $gg\to b\bar{b}$ fusion subprocesses. We will closely follow the notation and formulas of Ref. 6 and use for the mass of the b quark $m_b=4.5$ GeV. For the upper limit in the mass integral over the Υ resonances, as required by this duality approach,[7] we use[6] $m'=5.3$ GeV. In Fig. 3 we show our predictions for $Bd\sigma/dy$ at center-of-mass rapidity $y=0$ for Υ production off nuclear targets using proton and pion beams. The normalization

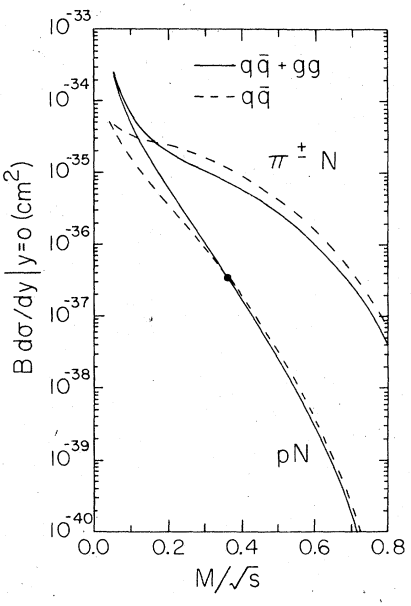

FIG. 3. The excitation curves for pion and proton induced Υ production from an isoscalar target at center-of-mass rapidity $y=0$. The $q\bar{q}$ ($q\bar{q}+gg$) predictions are shown by dashed (solid) lines. In each case the predictions have been normalized to the 400-GeV/c data point[1] shown.

corresponds to the single Gaussian fit of Ref. 1, $\sigma(\Upsilon)=3.4\times10^{-37}$ cm^2, at $\sqrt{\tau}=m_{\mu^+\mu^-}/\sqrt{s}=0.357$ where $m_{\mu^+\mu^-}=(Q^2)^{1/2}$. We have chosen to give the predictions for the entire Υ peak, even though it most probably consists of several unresolved states, because experiments with modest statistics will in fact only be able to measure this single peak. The results are shown for both the $\pi^{\pm}$ and p initiated reactions with the normalization for the $\pi^{\pm}$ curve determined by that of the p curve. The curves shown in Fig. 3 were obtained using the dynamical QCD distributions of Sec. II B; similar results were obtained using the counting-rule distributions. The dashed curves show the results of keeping only the $q\bar{q}$ fusion subprocess while the solid curves show the results of adding the gluon-gluon fusion contribution. The slope of the excitation curve for the proton case is significantly steeper in the region $m/\sqrt{s}\lesssim0.3$ after the addition of the gluon term. At $\sqrt{s}=60$ GeV ($\sqrt{\tau}=0.16$), corresponding to the upper end of the CERN ISR energy range, this increases the cross section by about a factor of 2. Thus the rapid upward sweep due to the increasing gluon-gluon fusion term should be observable using existing facilities. A similar set of curves is predicted for J/ψ production, but there are quantitative differences due to the presence of the scaling deviations in the parton distribution functions. For very small values of x the parton distributions increase with increasing Q^2, whereas at large x values they decrease. Thus the slope of the J/ψ excitation curve is flatter. In this model the relative normalization of the J/ψ and Υ curves is unspecified. However, if the curves were normalized at $\sqrt{\tau}=0.4$ in order to compare slopes, then the $q\bar{q}+gg$ curve for $pN\to J/\psi+X$ would lie about a factor of 1.5 below the corresponding Υ curve at $\sqrt{\tau}=0.05$.

For the proton beam case the $q\bar{q}$ term is given by the product of a sea and a valence term. Thus the gg and $q\bar{q}$ terms are comparable over a significant portion of the τ range shown. On the other hand, the pion reaction is dominated by a valence-valence interaction so that the gluon term makes a sizable contribution only for $m/\sqrt{s}\lesssim0.15$. The shift in the pion $q\bar{q}$ curve at larger $m/\sqrt{s}$ values is solely due to the change in the proton-curve normalization.

In Fig. 4 the predicted x_F distributions for both $\pi^{\pm}$ and p initiated reactions on isoscalar targets are shown.[14] Figure 4(a) [4(b)] corresponds to the dynamical QCD (counting-rule) distributions. In each case the gluon contribution to the proton reaction is significant at small x_F and decreases more rapidly with increasing x_F than does the flatter $q\bar{q}$ contribution. Note, however, that the fractional contribution from the gluon-gluon fusion is smaller than was the case for J/ψ production.[6] This is a result of the fact that the gluon distribution decreases more rapidly with increasing Q^2.

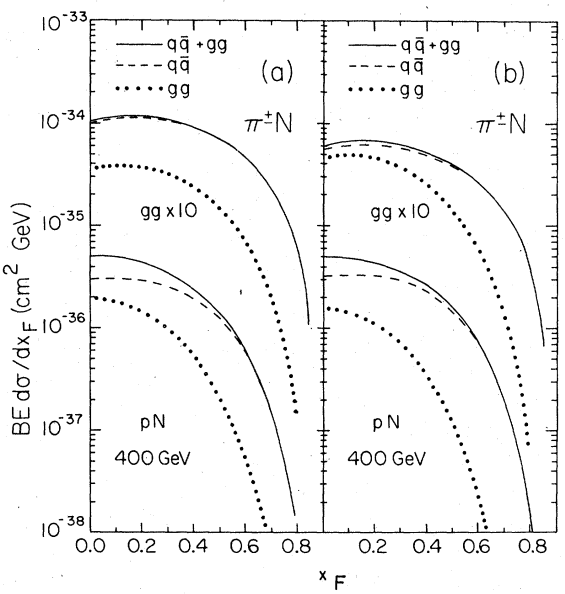

FIG. 4. The x_F distributions, $BEd\sigma/dx_F$, for Υ production using $\pi^{\pm}$ and p beams with an isoscalar target calculated using (a) the dynamical QCD parton distributions, (b) the counting-rule parton distributions. For both cases the $q\bar{q}+gg$ curve has been normalized to the $x_F=0$ pN data point at 400 GeV/c (see Ref. 1).

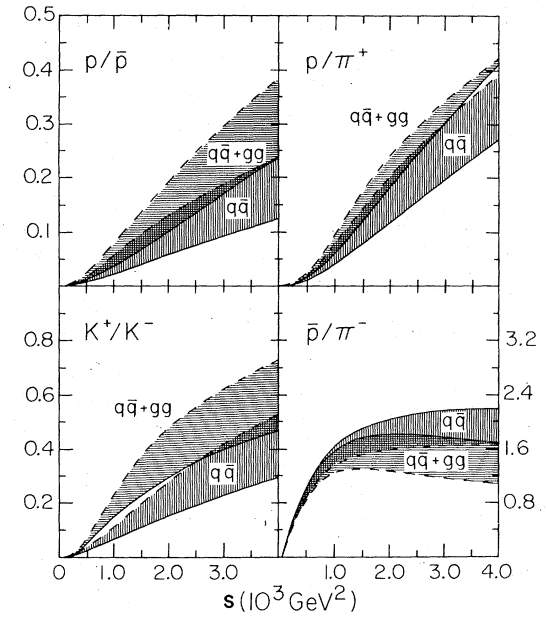

FIG. 5. Predictions for the Υ total-cross-section ratios using p, $\bar{p}$, $\pi^{\pm}$, and $K^{\pm}$ beams on an isoscalar target. In each case the solid curve was obtained using the dynamical QCD distributions while the dashed curve corresponds to the counting-rule distributions.

than does the sea, as can be seen in Figs. 1 and 2. For the pion case the gluon plays virtually no role since it is totally dominated by the valence-valence interaction in the $q\bar{q}$ term. The resulting x_F predictions are very flat, with a significant decrease occurring only for $x_F \gtrsim 0.4$. As a result of the dominance of the $q\bar{q}$ component the x_F dependence of the Υ and the $\mu^+\mu^-$ background should be similar, assuming that the continuum is produced via the Drell-Yan mechanism. However, when gluon effects are important, as in the proton case, the resonance signal-to-background ratio should decrease slightly with increasing x_F since the $q\bar{q}$ component is flatter than the gg term.

In Fig. 5 are shown the predictions for the $p/\bar{p}$, p/π^+, K^+/K^-, and $\bar{p}/\pi^-$ cross-section ratios for Υ production from an isoscalar target with $x_F \geq 0$. The K^+ and K^- valence, sea, and gluon distributions are assumed to be equal to the corresponding pion distributions as suggested by local SU(3) symmetry.[8] In each case the solid (dashed) curves were obtained using the dynamical QCD (counting-rule) parton distributions. The results shown here for Υ production are similar to those shown for J/ψ production in Fig. 8 of Ref. 6 but with the corresponding value of s increased by a factor of 10 such that the value of $\sqrt{\tau}$ is unchanged. Indeed, in the absence of scaling violations in the parton distribution functions the results for Υ and J/ψ production at fixed τ would be identical.[15] However, as shown in Figs. 1 and 2, there exists substantial Q^2 dependence in the various distributions, the most pronounced being for the gluon. The sizable decrease in the gluon distributions somewhat dilutes the effect of the gluon-gluon fusion term so that the two shaded bands show a greater region of overlap for Υ than for J/ψ production. This increased overlap shows that in fact the ambiguity stemming from the uncertainty in the input parton distribution functions is, in some instances, comparable to the shift caused by adding the gluon-gluon contribution.

Of particular interest is the p/π^+ ratio since in the currently accessible energy range, $p_{\text{lab}} \lesssim 500$ GeV, the gain in cross section can be more than 2 orders of magnitude if a pion rather than proton beam is used. A significant increase in cross section can also be obtained with the use of a $\bar{p}$ beam.

The results of this analysis show that the inclusion of the gluon-gluon fusion term in addition to the more conventional $q\bar{q}$ annihilation term results in the same qualitative behavior for Υ and J/ψ production at fixed values of τ. However, the larger Q^2 value for Υ production results in some quantitative differences due to the scaling violations in the parton distribution functions. In particular, the rapid decrease with increasing Q^2 of the pion and nucleon gluon distributions results in a diminution of the gluon effects for higher mass states. Therefore, the study of production ratios as a test for the presence of gluon effects would best be done with J/ψ production. On the other hand, for sufficiently small values of $\sqrt{\tau}$ the gluon distributions actually increase with increasing Q^2 as shown in Figs. 1 and 2. Thus, as the energy is increased, the Υ cross section becomes increasingly larger than that predicted by the $q\bar{q}$ subprocess alone. This predicted rise is a clear signal of the presence of the gluon-gluon subprocess.

ACKNOWLEDGMENT

One of us (E.R.) would like to thank M. Glück for many helpful discussions. This work was supported in part by the U. S. Department of Energy.

*Permanent address: Institut für Physik, Universität Mainz, 6500 Mainz, West Germany.

[1]S. W. Herb *et al.*, Phys. Rev. Lett. 39, 252 (1977).
[2]E. Eichten and K. Gottfried, Phys. Lett. 66B, 286 (1977).
[3]J. Ellis, M.K. Gaillard, D. V. Nanopoulos, and S. Rudaz, Nucl Phys. B 131, 285 (1977).
[4]M. Kobayashi and K. Maskawa, Prog. Theor. Phys. 49, 652 (1973).
[5]S. Nandi, University of Bonn Report No. HE-77-27, 1977 (unpublished).
[6]M. Glück, J. F. Owens, and E. Reya, Phys. Rev. D 17, 2324 (1978).
[7]H. Fritzsch, Phys. Lett. 67B, 217 (1977).
[8]G. R. Farrar, Nucl. Phys. B77, 429 (1974); J. F. Gunion, Phys. Rev. D 10, 242 (1974).
[9]G. Parisi and R. Petronzio, Phys. Lett. 62B, 331 (1976).
[10]M. Gluck, and E. Reya, Nucl. Phys. B 130, 76 (1977).
[11]A. J. Buras and K. J. F. Gaemers, Nucl. Phys. B132, 249 (1978).
[12]The counting-rule nucleon distributions use $Q_0^2 = 1.8$ GeV^2 since the valence parametrization is that of Ref. 11. However, for the remaining distributions presented here, $Q_0^2 = 3$ GeV^2.
[13]M. Glück and E. Reya, Phys. Rev. D 16, 3242 (1977).
[14]For an isoscalar target the π^+ and π^- predictions are identical.
[15]The counting-rule nucleon sea used here is flatter than that used for the naive parton model in Ref. 6. This causes a slight upward shift of the dashed $q\bar{q}$ lines.